JOURNAL OF SPACECRAFT AND ROCKETS
Vol. 32, No. 3, May–June 1995

Simulated Rarefied Entry of the Galileo Probe into the Jovian Atmosphere

Brian L. Haas* and Frank S. Milos†
NASA Ames Research Center, Moffett Field, California 94035-1000

Flowfield properties and aerodynamics are computed with a direct simulation Monte Carlo method in the rarefied flow regime during entry of the Galileo Probe into the atmosphere of Jupiter. The objective is to predict accurately the vehicle's drag coefficient, which is needed to assess atmospheric properties from the onboard atmospheric structure experiment, where highly sensitive accelerometers will measure the drag effects to within 10^{-5} m/s^2 during the initial entry phase at high altitudes. The corresponding flow rarefaction extends from the free-molecule limit to the near-continuum transition regime ($Re_\infty < 1000$). Simulation results, employing a simple radiative equilibrium surface model, indicate that C_D varies from 2.1 at the free-molecule limit down to 1.6 at $Re_\infty = 1000$. Results compared very well to those from ballistic-range experiments. Detailed material response of the carbon–phenolic heat shield was then coupled directly into the DSMC code to account accurately for conductivity, heat capacity, and pyrolysis, and the simulations were repeated. The predicted pyrolysis mass efflux was 8–14 times higher than the incident freestream mass flux and had significant effects on the drag.

Nomenclature

A = thermal accommodation coefficient
B = constant in decomposition rate, s^{-1}
C = pyrolysis species mass densities, kg/m^3
C_D = drag coefficient
c_p = heat capacity of solid material, J/kg · K
D = probe diameter
d = particle diameter
E = pyrolysis activation temperature, K
g_j = degeneracy of rotational quantum level j
h = enthalpy, J/kg
j = rotational quantum level
k = Boltzmann constant, 1.3805×10^{-23} J/K
Kn = Knudsen number
M = Mach number
m = pyrolysis-gas mass efflux, kg/m^2 · s
N_d = number of pyrolysis decomposition reactions
q = net convective heat flux, W/m^2
Re = Reynolds number based on diameter
r_j = normalized rotational energy of level j
s = arc length along surface, m
T = temperature, K
t = time during entry ($t = 0$ s at 735 km)
x = position relative to stagnation point, m
y = normal distance into surface material, m
Z = collision number for internal relaxation
α = exponent of intermolecular potential
δ = material thickness, m
ε = material radiative emissivity
ζ_r = number of rotational degrees of freedom
η = decomposition reaction order
θ = characteristic mode temperature, K
μ = viscosity, kg/m · s
ρ = mass density, kg/m^3
ϱ = dimensionless pyrolysis mass density
σ = Stefan–Boltzmann constant, 5.67×10^{-8} W/(m^2 · K^4)
χ = pyrolysis interpolation fraction

Subscripts

c = char material
D = deep-space value
g = pyrolysis gas
i = decomposition species i
ref = reference value
r = rotational mode
s = solid-phase material
v = vibrational mode
w = value at wall or surface
κ = attributed to conductivity
∞ = freestream value

Presented as Paper 94-2043 at the AIAA/ASME 6th Thermophysics and Heat Transfer Conference, Colorado Springs, CO, June 20–23, 1994; received Aug. 15, 1994; revision received Dec. 5, 1994; accepted for publication Dec. 8, 1994.

*Research Scientist, Thermosciences Institute, M/S 230-2. Member AIAA.
†Research Scientist. Member AIAA.

Introduction

JUST prior to encountering and orbiting Jupiter in December 1995, the Galileo spacecraft will release a probe that will enter the Jovian atmosphere. During the initial aerobraking phase, the 45-deg blunted-cone probe will be protected by a carbon–phenolic heat shield. Once the probe velocity has been reduced from 47.5 to 0.74 km/s, and entry heating has diminished, the probe will eject its heat shield and deploy a parachute. During descent, the probe will make several in situ measurements of atmospheric properties and transmit those data to the orbiting spacecraft. However, an atmospheric structure experiment,[1] similar to that employed in the Pioneer Venus and Mars Viking missions,[2] will also be on the Galileo probe to measure deceleration during the high-altitude entry phase. This experiment deduces atmospheric density, pressure, and temperature from deceleration measurements so long as the vehicle drag coefficient is known a priori. The instrument is sufficiently sensitive to detect deceleration exceeding 10^{-5} m/s^2. Consequently, meaningful properties can be assessed for the Jovian upper atmosphere where the probe encounters highly rarefied flow during entry prior to peak heating and ablation of the heat shield. This flow regime is bounded by the effective free-molecule limit at 750-km altitude ($Re_\infty = 0.1$) and the near-continuum limit at 350 km ($Re_\infty = 1000$). Note that since Jupiter has no identifiable surface, altitude is measured relative to the 1.0-bar pressure level in the Jovian atmosphere.

Accuracy of the experiment, however, depends upon the accuracy with which the probe drag coefficient is determined. Intrieri and Kirk[3] conducted a series of experiments in the ballistic-range facilities at NASA Ames Research Center to measure the drag of several blunt-body configurations, including the Pioneer Venus and Galileo probes. Results for each were very similar, leading to the values near $C_D = 1.1$ for $Re_\infty > 1000$. However, C_D rises significantly (approaching values near 2.0) for decreasing Re_∞ below

1000, although Intrieri's experiments did not give results in the rarefied regime. Furthermore, the experimental surface materials, gas species, and flow conditions (Mach number, density, gas composition, etc.) differed significantly from those anticipated for Galileo probe entry.

Because of the lack of sufficient experimental data, the probe aerodynamics must be estimated computationally. Unfortunately, the flow regime is ill suited to simulations that are based upon the continuum Navier–Stokes equations, owing to limitations in constitutive relations for heat flux and shear stress. Instead, highly rarefied flows, for which the ratio of the molecular mean free path to a body dimension is large (Knudsen number $Kn > 0.10$), are best simulated computationally using direct simulation Monte Carlo (DSMC) particle methods.[4,5] In DSMC, the gasdynamics are modeled directly by the motion and interaction of thousands or millions of discrete particles. Particles that strike the vehicle may reflect back into the flow with velocities and internal energies corresponding to full or partial accommodation to the surface. The simulation permits accurate assessment of vehicle aerodynamics, heating, and properties of the flowfield at low densities.

The objective of the present study was to assess the drag coefficient for the Galileo probe during entry from 750-km down to 350-km altitude in the Jovian atmosphere. Because of uncertainties in the applicable surface thermal accommodation coefficient, simulations were repeated using different values to quantify its effects upon the vehicle entry. All simulations initially employed a simple radiative-equilibrium model for gas–surface interactions. However, excessive heating, even under rarefied conditions, will likely cause the heat shield to pyrolyze, ejecting gas into the flow from the surface. To capture this behavior accurately, simulations were repeated using new surface models, which allowed for transient convective heating, radiation, in-depth conduction, heat capacity, and the flow of pyrolysis gases through the porous material. By coupling material response directly into its surface model, the new DSMC code simulates the entry environment and predicts vehicle aerodynamics as required for this and other aerobraking missions.

Simulation Models

The DSMC code employed in the present study was developed by Baganoff and McDonald[5,6] and enhanced for better application to rarefied aeropass maneuvers.[7] The flowfield is divided into cubic Cartesian cells to facilitate selection of colliding particles and sampling of macroscopic flow properties. A body geometry is modeled by a composite of planar facets in those cells through which the body surfaces pass. Each surface facet collects statistics regarding momentum and energy flux and may assume a surface temperature independent of neighboring facets. To simulate entry with the DSMC method, one must first specify properties of both gas–gas and gas–surface interactions.

Gas–Gas Interaction Model

Molecular interaction is simulated by the variable hard-sphere (VHS) model of Bird,[8] in which the collision outcome corresponds to isotropic scattering, akin to the mechanics of hard-sphere interactions. The collision rate, however, corresponds to an inverse power-law intermolecular potential of exponent α. This parameter must be specified between the limits of the Maxwell molecule ($\alpha = 4$) and the hard sphere ($\alpha = \infty$), and can be estimated from the known temperature dependence of the gas viscosity, μ as follows:

$$\frac{\mu}{\mu_{\text{ref}}} = \left(\frac{T}{T_{\text{ref}}}\right)^{\frac{1}{2}+(2/\alpha)} \tag{1}$$

Transport properties of the Jovian atmosphere, thought to be composed of a mixture of 89% H_2 and 11% He, were calculated from kinetic theory of Biolsi.[9] That work employed sophisticated semiempirical interaction potentials to evaluate the detailed collision integrals for viscosity, thermal conductivity, and binary diffusion for the gas mixture. Biolsi's results for viscosity are plotted in Fig. 1 and compared with curves corresponding to the VHS model. The VHS parameters that yield best agreement in the figure and were employed in the current work are given by $\mu_{\text{ref}} = 2.24 \times 10^{-5}$ kg/m · s, $T_{\text{ref}} = 1000$ K, and $\alpha = 10.5$. These parameters led to particle reference diameters[10] of $d_{\text{ref}} = 2.51$ Å, assumed equal for H_2 and He in the present work.

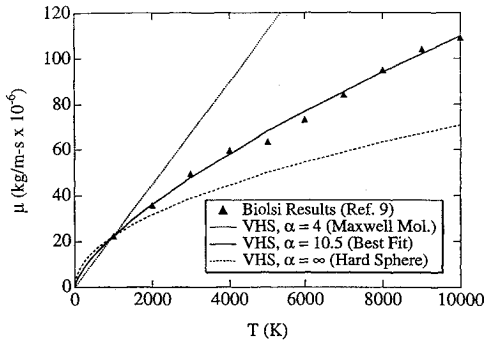

Fig. 1 Viscosity of the H_2–He Jovian atmosphere.

Internal-Energy Exchange Model

Of additional concern in gas–gas interactions is the inelastic exchange of molecular energies due to relaxation of the internal energy modes for rotation and vibration. The mechanics of these exchange processes are modeled in the DSMC code by the methods of Borgnakke and Larsen[11] and Haas et al.[12] These involve partitioning postcollision thermal energies in a manner that corresponds to equilibrium distributions. The rates of rotational and vibrational relaxation are dictated by collision numbers Z_r and Z_v, respectively. Solutions of the master equation using state-to-state transition probabilities estimated from quasiclassical methods[13–15] have led to rotational relaxation rates in H_2 described by $Z_r = 100$. Simple application of the Millikan and White's[16] empirical expression for vibrational relaxation rates suggests that Z_v is several orders of magnitude larger than Z_r, leading to exceedingly slow vibrational excitation. Furthermore, given the high characteristic temperature of vibration[13] ($\theta_v = 6320$ K) for H_2, it is unlikely that the vibrational mode will contribute significantly to the thermophysics of this flow, so it was neglected in the present work.

DSMC methods typically model diatomic molecular rotation as a continuous-energy mode with two degrees of freedom, $\zeta_r = 2$. However, at freestream conditions, the quantized nature of the rotational mode for H_2 leads to an effective number of degrees of freedom below two as a result of its high characteristic temperature[17] ($\theta_r = 85.33$ K). As plotted in Fig. 2, the dependence of ζ_r upon temperature T is described by the rotational partition function and may be expressed as follows:

$$\zeta_r = 2\frac{\sum_j g_j r_j \exp(-r_j)}{\sum_j g_j \exp(-r_j)} \tag{2}$$

where the normalized energy r_j and degeneracy g_j per rotational quantum level j are defined[18] by

$$r_j = j(j+1)(\theta_r/kT) \tag{3}$$

$$g_j = 2j + 1 \tag{4}$$

Rather than incorporate a detailed model of the quantized rotational mode into the code, a simpler adaptation of the continuous-energy model was employed here. First, it was recognized that collisions promoting rotational excitation will occur predominantly in the high-temperature regions of the flow. Since the rotational degrees of freedom would become fully excited in those regions, the normal Borgnakke–Larsen model for exchange mechanics was employed, assuming $\zeta_r = 2$. However, since the freestream temperature was fairly low, incoming particles were initialized so that the mean rotational energy was given by $\zeta_r kT/2$, where $\zeta_r < 2$ is evaluated from Eq. (2). This prevents the freestream from being too energetic in rotation, as would occur if initialized with $\zeta_r = 2$. A similar procedure was used to define the internal energy of H_2 molecules reflecting diffusely from the vehicle surface, since some of the surface temperatures were low.

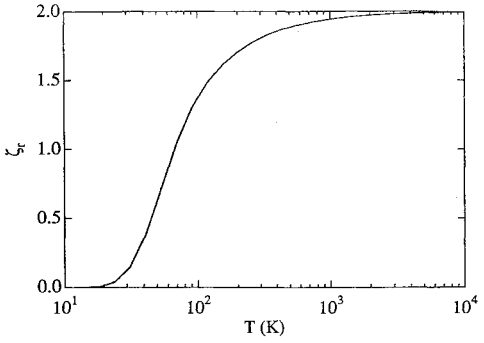

Fig. 2 Temperature dependence of the rotational degrees of freedom for H_2.

Gas–Surface Interaction Model

Details regarding the interaction of gas molecules with surfaces are not well understood in general, and are dependent upon several factors, including surface roughness, impact dynamics, molecular potentials, and thermal energies. However, simple engineering models often suffice to simulate gas–surface interaction phenomena. In the present work, a single thermal accommodation coefficient A describes the fraction of particles that accommodate fully to the surface versus those which reflect specularly. Full accommodation implies diffuse reflection of the particle from the surface with thermal energy corresponding to the surface wall temperature T_w. Rather than prescribe a temperature for the surface, the code couples a simple surface heat transfer model into the flow solution to compute T_w directly.[19,20] This model assumes that each surface facet is in radiative equilibrium with space at temperature $T_D = 150$ K, leading to the energy balance given by

$$q - \varepsilon\sigma\left(T_w^4 - T_D^4\right) = 0 \tag{5}$$

Here, q is the net convected heat flux to each facet, including both incident and reflected energy. As will be described in the next section, this model can be enhanced to account for material heat capacity, thermal conduction through the heat shield, and pyrolysis of the surface material.

Definitive values for A and ε for the interaction of Jovian atmospheric gases upon carbon–phenolic material at flight conditions are not readily available. A surface emissivity of $\varepsilon = 0.85$ was suggested by Bueche[21] from ground-based experiments, flight data, and theoretical predictions, and is used here because it is consistent with estimates cited elsewhere.[22–25] Appropriate values for A have even more uncertainty than ε; only limited related experimental data[26] and theoretical[27] results were found. Therefore it was necessary to repeat simulations using different values of A to assess the sensitivity of the results to this parameter.

Coupled Model for Material Response

Because of the high entry velocity of the Galileo probe, even in the rarefied regime, surface heating will be great enough to cause the carbon–phenolic heat shield to pyrolyze, thus emitting gas molecules into the flow. This behavior can, in turn, affect the vehicle aerodynamics significantly. As an improvement on the assumption above that the surface is in radiative equilibrium, the dynamic response of the surface material can be calculated by coupling routines from the Charring Material Thermal Response and Ablation (CMA) program[28,29] directly into the DSMC code. CMA is a finite-difference procedure for computing one-dimensional transient energy transport within a thermal protection material that can ablate from a heated surface and can decompose in depth. This section briefly describes CMA models used in this work.

When heated, many TPS materials experience a series of chemical reactions that release gaseous byproducts. Upon completion of these reactions, the porous residual "char" that remains has lower density than the original "virgin" solid. These charring materials are modeled as a sum of constituents, each of which decomposes independently according to an Arrhenius reaction-rate expression. The decomposition equations can be written

$$\rho_s = \rho_c + \sum_{i=1}^{N_d} C_i \varrho_i \tag{6}$$

$$\frac{\partial \varrho_i}{\partial t} = -B_i e^{-E_i/T} \varrho_i^{\eta_i} \tag{7}$$

where ρ_c is the char density, ϱ_i are dimensionless constituent densities, N_d is the number of decomposition reactions (typically 2 or 3), and the parameters B_i, E_i, and η_i are decomposition rate coefficients. The constituent densities decrease from unity to zero as the reactions proceed. The original virgin density is $\rho_v = \rho_c + \sum C_i$. Decomposition rate parameters have been determined experimentally for the carbon–phenolic heat-shield material.

The properties of the solid are functions of both density and temperature. In practice, properties are tabulated as functions of temperature and pressure for the virgin material and for the fully charred material. For a partially charred state the effective solid properties are found by interpolation. For example, the solid heat capacity is

$$c_{ps}(\rho_s, T) = \chi c_{pv}(T) + (1 - \chi) c_{pc}(T) \tag{8}$$

where

$$\chi = \frac{\rho_v}{\rho_v - \rho_c}\left(1 - \frac{\rho_c}{\rho_s}\right) \tag{9}$$

Pyrolysis gas is assumed to be in local thermodynamic equilibrium with the solid. Therefore, energy transport is governed by a single equation,

$$\rho c_p \frac{\partial T}{\partial t} = \frac{\partial}{\partial y}\left(k \frac{\partial T}{\partial y}\right) + m_g \frac{\partial h_g}{\partial y} + (h_g - h_s)\frac{\partial \rho_s}{\partial t} \tag{10}$$

which takes into account local energy accumulation, heat conduction, enthalpy convection, and heat of pyrolysis. The y coordinate points into the solid in the surface-normal direction. The variable m_g is the superficial pyrolysis-gas mass flux in the outward direction. For quasisteady flow, material thickness δ, and an impermeable back wall, the mass flux is obtained from

$$m_g = \int_\delta^y \frac{\partial \rho_s}{\partial t}\, \mathrm{d}y \tag{11}$$

The equation set is completed by specification of two boundary conditions for the energy equation. The interior surface was assumed to be insulated. At the heated surface, the surface energy balance takes the simple form

$$q - \varepsilon\sigma\left(T_w^4 - T_D^4\right) - q_k = 0 \tag{12}$$

where q is the total kinetic energy imparted to the surface by reflecting particles. This energy is either radiated to space or conducted into the solid. The pyrolysis mass efflux, m_{gw}, does not appear explicitly in Eq. (12); however, mass injection strongly affects q by reducing the number and velocity of particles striking the surface. The model in Eq. (12) does not include radiation to the probe surface from the flow environment, nor does it attempt to take accurate account of the influence of the planet on the effective deep-space temperature. However, these sources of radiation would be extremely small relative to convection and conduction, and therefore do not warrant detailed treatment here.

The DSMC code simulates the flow at a single instant in time only. However, calculations at a sequence of altitudes along the flight trajectory provide the transient surface heat flux $q(t)$ for each surface facet on the model vehicle. The CMA routine marches Eqs. (6–10) in time along the trajectory to obtain the history of all surface quantities, including T_w and m_{gw}, for each facet. The DSMC code then uses these values to eject new pyrolysis particles from each surface facet accordingly. These particles, in turn, transport energy and

momentum from the surface into the flow. Since q depends to some extent on T_w and highly on m_{gw}, the CMA routine is called upon periodically during the DSMC calculation to update the values of T_w and m_{gw} for each facet. In this manner, the DSMC code coverges to a steady solution for the current time point in the trajectory.

It should be noted that pyrolysis products are a mixture of chemical species containing the elements hydrogen, carbon, and oxygen, including H_2, CO, CH_4, C_6H_6, and other minor hydrocarbons. At the low pressures and sufficiently low surface temperatures (below 2000 K) considered in this work, the diatomic molecules H_2 and CO are the predominant species. Therefore, in the DSMC calculations the pyrolysis gas is modeled as a mixture of $\frac{2}{3}$ H_2 molecules and $\frac{1}{3}$ CO molecules. This mixture provides the correct amount of H_2 and a reasonable approximation to the average molecular weight of the pyrolysis gas. Parameters for the VHS potential for CO were found in the same manner as for the H_2–He mixture from Eq. (1). Using results of viscosity calculations by Hilsenrath et al.,[30] best agreement corresponds to $\mu_{\text{ref}} = 2.22 \times 10^{-5}$ kg/m · s, $T_{\text{ref}} = 400$ K, $\alpha = 10.5$, and a particle reference diameter of $d_{\text{ref}} = 3.79$ Å, for CO.

Simulation Results

The DSMC code was used to simulate entry of the Galileo probe at several points along its trajectory from 735-km to 353-km altitude. Table 1 lists the simulation conditions for each case with atmospheric data taken from Orton. Note that time is measured relative to the 735-km trajectory point. For all cases the velocity was assumed to be 47,450 m/s, consistent with the planned entry trajectory, and the Knudsen number and Reynolds number were based on the probe diameter (1.265 m). The grid resolution employed here is defined in Table 1 by the size of the probe diameter measured in cell lengths, and was sufficiently fine to yield less than 1% error in drag and heating.[31] The geometry of the probe is compared with the simulation models in Fig. 3. Only one quadrant of the probe was simulated, taking advantage of two planes of symmetry of the body. These results employed the radiative equilibrium surface model neglecting pyrolysis. The effects of including pyrolysis and detailed material response are presented in the next section.

In general, flows with greater Re_∞ require greater resolution in order to resolve flow gradients and avoid overpredicting drag and heat transfer. However, the required size of the flow domain increases with lower Re_∞ because molecules that reflect from the probe's surface are capable of diffusing far into the flow when collisions are infrequent. The extent of the upstream diffusion of particles is depicted in the plot of gas temperature along the stagnation streamline in Fig. 4. The upstream domain boundary for each simulation case was sufficiently far upstream that the translational temperature was near its freestream value, to prevent overprediction of heat transfer and drag.[31] Density profiles along the stagnation streamline are plotted in Fig. 5 and also exhibit the effects of rarefaction. Note that no clear shock structure is observed, since the shock is fully merged with the body layer. The density rose considerably near the relatively cool body surface on account of particle reflection with low kinetic energy.

For each case, the simulation employed at least 16 particles per cell in the freestream and roughly 3 to 7 million particles total. The code was optimized for vector processing on Cray supercomputers, requiring roughly 0.6 μs/particle · timestep on the Cray C-90 or a total run time of 5000–8000 CPU seconds, depending upon the case. Memory requirements ranged from 50 to 200 megawords.

Results Neglecting Pyrolysis

Results of each case, identified by Re_∞, are presented in Table 2. The cases were run with $A = 0.75$, and several were repeated with $A = \{0.5, 0.9\}$. Heating of the nose region was highly sensitive to the accommodation coefficient A, whereas drag was fairly insensitive, particularly for the highest and lowest Re_∞. Simulated drag coefficients for the Galileo probe are plotted in Fig. 6 and compared with the experimental ballistic-range results of Intrieri and Kirk[3] for

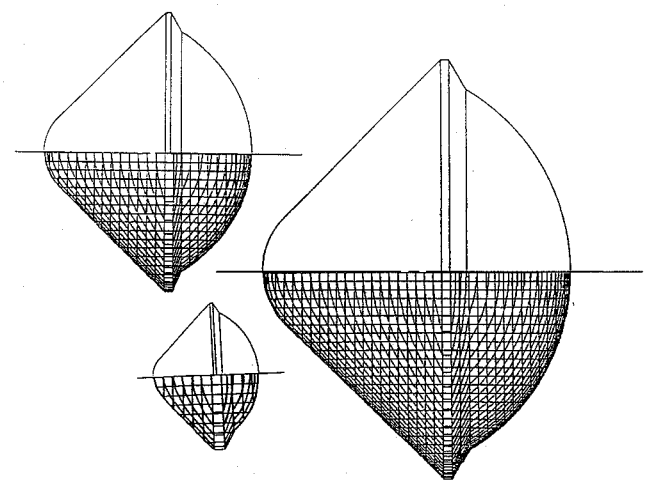

Fig. 3 Comparisons of probe geometry to simulation configurations employing differing resolutions.

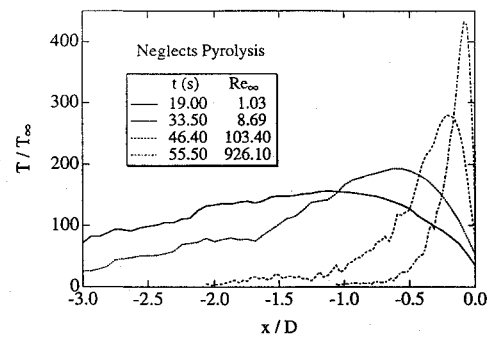

Fig. 4 Translational temperature along the stagnation streamline.

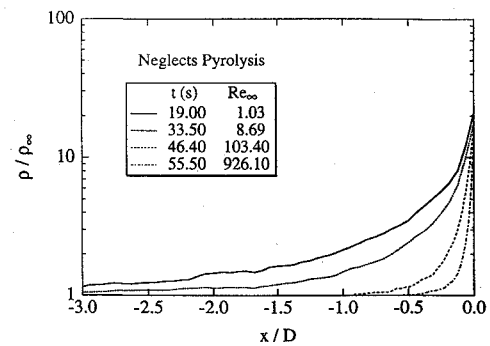

Fig. 5 Mass density along the stagnation streamline.

Table 1 Galileo probe entry simulation conditions

t, s	Alt., km	Re	M	Kn	T, K	ρ, kg/m^3	D, cells
0.00	735	0.10	31.47	415.59	425.0	2.024×10^{-11}	16
19.00	604	1.03	34.15	43.01	360.5	1.896×10^{-10}	16
33.50	506	8.69	37.20	5.55	303.2	4.422×10^{-9}	16
41.00	453	34.01	39.61	1.51	267.0	5.100×10^{-9}	16
46.40	416	103.41	41.86	0.53	238.7	1.435×10^{-8}	32
51.25	382	322.47	44.58	0.18	210.0	4.097×10^{-8}	32
55.50	353	926.15	46.35	0.07	194.0	1.114×10^{-7}	48

Table 2 Galileo probe entry simulation results

Re	A	C_D	q_{nose}, W/m^2	T_{nose}, K
0.10	0.75	2.06	7.66×10^2	358
1.03	0.75	2.05	6.49×10^3	602
8.69	0.75	2.02	4.87×10^4	998
34.01	0.75	1.97	1.69×10^5	1,370
103.41	0.75	1.90	4.49×10^5	1,740
322.47	0.75	1.78	1.20×10^6	2,240
926.15	0.75	1.63	2.98×10^6	2,800
0.10	0.50	2.06	$4.74E \times 10^2$	319
8.69	0.50	2.05	$3.26E \times 10^4$	910
103.41	0.50	1.93	$3.10E \times 10^5$	1,580
926.15	0.50	1.63	$2.09E \times 10^6$	2,550
0.10	0.90	2.04	$8.48E \times 10^2$	367
8.69	0.90	2.01	$5.79E \times 10^4$	1,050
103.41	0.90	1.86	$5.29E \times 10^5$	1,830
926.15	0.90	1.65	$3.56E \times 10^6$	2,930
34.01	pyrol	1.96	$1.67E \times 10^5$	482
103.41	pyrol	1.97	$3.42E \times 10^5$	642
322.47	pyrol	1.69	$3.75E \times 10^5$	897
926.15	pyrol	1.41	$7.11E \times 10^5$	1,130

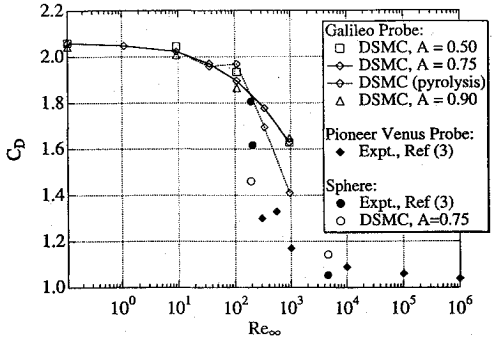

Fig. 6 Drag coefficients from DSMC simulations and experiments.

spheres and the Pioneer Venus probe. Unfortunately, their results for the Galileo probe, also in Ref. 3, were all at high angles of attack and were of questionable quality at low Re_∞.

In general, the drag coefficient decreased with increasing Re_∞ above 10, but did not appear to blend well with the high-Re_∞ experimental data. However, the experiments were performed at lower Mach numbers (roughly $M_\infty = 14.5$) in CO_2, rather than the high Mach numbers expected for Galileo entry in the H_2–He Jovian atmosphere. Indeed, for comparing highly rarefied flows, a suitable parameter for correlating the data would be the Knudsen number Kn_∞. Replotting the data in Fig. 7 suggests a smoother transition between the simulation results and the experimental data.

It was instructive to simulate a few Intrieri and Kirk's experiments for more direct comparison. Spheres flying at roughly $M_\infty = 14.5$ in pure CO_2 for $Re_\infty = \{192, 4564\}$ were simulated with the DSMC code, employing the same surface description as above. The results are included in the drag plots and appear to follow the experimental trends quite well.

Results Including Pyrolysis

The DSMC calculations above employed a radiative-equilibrium energy balance to compute the surface temperature. This boundary condition neglects any effects of heat capacitance and heat conduction in the spacecraft heat shield and therefore provides an upper bound for the surface temperature. The calculations also neglected pyrolysis from the heat shield, which can be significant for a high-energy incident flow at very low densities.

To assess the effects of surface pyrolysis quantitatively, the simulations above were repeated using the CMA routines coupled into the DSMC code as described above. Temperature-dependent material properties, surface reradiation, and in-depth pyrolysis were included in the calculation, but surface ablation was neglected. The initial surface temperature was estimated to equal the deep-space temperature of 150 K uniformly over the vehicle just prior to atmospheric entry. For each pyrolysis case the accommodation coefficient was set to $A = 0.75$.

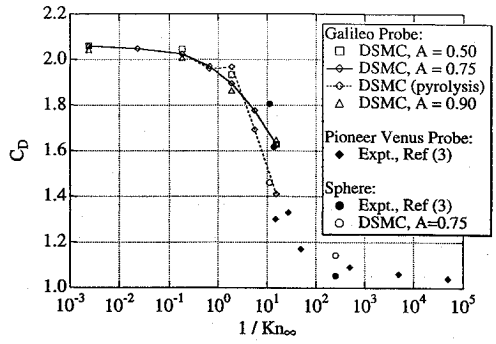

Fig. 7 Drag coefficients versus $1/Kn_\infty$.

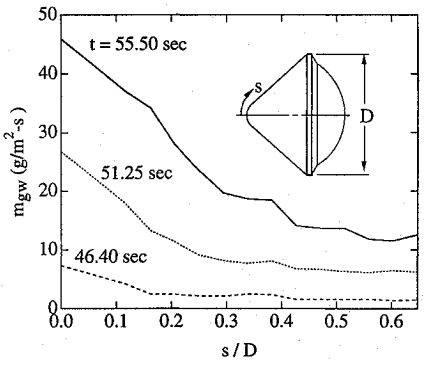

Fig. 8 Surface profiles of pyrolysis mass efflux at several trajectory points.

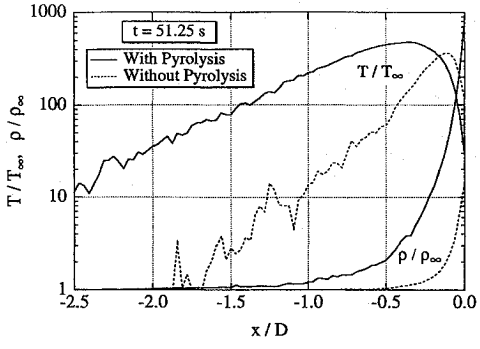

Fig. 9 Profiles of flow temperature and density along the stagnation streamline.

Surface pyrolysis was negligible for the first four trajectory points, but became very large for $t > 41.0$ s. Figure 8 presents profiles over the forebody surface of pyrolysis-gas mass flux at each of the last three trajectory points. As expected for each, the peak pyrolysis efflux occurred at the stagnation point ($s = 0$), reaching a maximum value that was 8–14 times the freestream mass flux impacting the vehicle.

As listed in Table 2, the surface temperature at the nose, as computed with coupled pyrolysis, was well below the radiative-equilibrium temperature. This was also observed at $t = 41.0$ s as a result of the conduction and heat capacity of the heat-shield material, even though pyrolysis was negligible at that time. Pyrolysis also led to considerably lower convective heat fluxes at the probe nose.

Profiles for flowfield translational temperature and mass density, when computed with and without pyrolysis, are compared in Fig. 9 for the trajectory point at $t = 51.25$ s. The pyrolysis emission forced the temperature to peak further upstream, and led to a lower stagnation temperature near the body surface than for the flow without pyrolysis. Particle emission and lower surface temperatures also increased the local fluid density near the body below that in simulations neglecting pyrolysis. A consequence of the observations

is that the DSMC simulation in the present work had to employ a larger upstream flow domain as well as finer grid resolution near the body in order to compute aerodynamics and heating accurately for pyrolyzing surfaces.

The resulting drag coefficients for these cases are included in Figs. 6 and 7. Whereas the transport of momentum due to the emission of pyrolysis products from the front of the vehicle tends to increase drag, the influence of this emission on the incoming flow tends to reduce the incident momentum imparted to the surface. Whether these competing effects would lead to a net increase or decrease in overall vehicle drag would be difficult to predict without performing simulations. Indeed, at $t = 46.4$ s the flow is sufficiently rarefied that the pyrolysis gas has very little influence on the incident flow, and the drag coefficient is greater than when pyrolysis is neglected. However, as flow density and pyrolysis emission increased in time, molecular collisions in front of the body caused a marked decrease in the convective heat transfer and the incident momentum flux, resulting in a lower drag coefficient for the last two trajectory points.

Conclusion

The drag on the Galileo probe during initial entry into the Jovian atmosphere was computed with a DSMC method, and the results were consistent with experimental data. However, the drag varies considerably with Reynolds numbers in the range $10 < Re_\infty < 10{,}000$ at the high-M_∞ flight conditions anticipated for the probe. Results correlate better with experiment when plotted against Knudsen number than against Reynolds number under highly rarefied conditions. Simple models for gas–gas and gas–surface interaction permitted efficient yet meaningful simulation of the flow, although the effects of significant surface pyrolysis warranted including more complex gas–surface models into the simulation. Uncertainties in the thermal accommodation coefficient A have minimal effect on the final results because of the insensitivity of drag to A, despite the great dependence of heating upon A.

Acknowledgments

This work was sponsored in part (for B.L.H.) by NASA Cooperative Agreement NCC2-582 with additional support to Eloret under NASA Contract NAS2-14031. The authors acknowledge and appreciate the support of NASA Ames Research Center and the Numerical Aerodynamics Simulation for use of their facilities.

References

[1]Seiff, A., Kirk, D. B., Young, R. E., Blanchard, R. C., Findlay, J. T., Kelly, G. M., and Sommer, S. C., "Measurement of Thermal Structure and Thermal Contrasts in the Atmosphere of Venus and Related Dynamical Observations: Results from the Four Pioneer Venus Probes," *Journal of Geophysical Research*, Vol. 85, No. A13, 1980, pp. 7903–7933.

[2]Seiff, A., and Kirk, D. B., "Structure of the Atmosphere of Mars in Summer at Mid-Latitudes," *Journal of Geophysical Research*, Vol. 82, No. 28, 1977, pp. 4364–4378.

[3]Intrieri, P. F., and Kirk, D. B., "High-Speed Aerodynamics of Several Blunt-Cone Configurations," *Journal of Spacecraft*, Vol. 24, No. 2, 1987, pp. 127–132.

[4]Bird, G. A., *Molecular Gas Dynamics*, 1st ed., Clarendon, Oxford, England, UK, 1976.

[5]Baganoff, D., and McDonald, J. D., "A Collision-Selection Rule for a Particle Simulation Method Suited to Vector Computers," *Physics of Fluids A*, Vol. 2, No. 7, 1990, pp. 1248–1259.

[6]McDonald, J. D., "A Computationally Efficient Particle Simulation Method Suited to Vector Computer Architectures," Ph.D. Thesis, Stanford Univ., Stanford, CA, 1989.

[7]Haas, B. L., and Feiereisen, W. J., "Particle Simulation of Rarefied Aeropass Maneuvers of the Magellan Spacecraft," *Journal of Spacecraft and Rockets*, Vol. 31, No. 1, 1994, pp. 17–24.

[8]Bird, C. A., "Monte-Carlo Simulation in an Engineering Context," *Rarefied Gas Dynamics*, edited by S. S. Fischer, AIAA, New York, 1981, Part I, p. 239.

[9]Biolsi, L., "Transport Properties in the Jovian Atmosphere," *Journal of Geophysical Research*, Vol. 83, No. A3, 1978, pp. 1125–1131.

[10]Bird, G. A., "Definition of Mean Free Path for Real Gases," *Physics of Fluids*, Vol. 26, No. 11, 1983, pp. 3222, 3223.

[11]Borgnakke, C., and Larsen, P. S., "Statistical Collision Model for Monte Carlo Simulation of Polyatomic Gas Mixture," *Journal of Computational Physics*, Vol. 18, No. 4, 1975, pp. 405–420.

[12]Haas, B. L., McDonald, J. D., and Dagum, L., "Models of Thermal Relaxation Mechanics for Particle Simulation Methods," *Journal of Computational Physics*, Vol. 107, No. 2, 1993, pp. 348–358.

[13]Sharma, S. P., and Schwenke, D. W., "Rate Parameters for Coupled Rotation–Vibration–Dissociation Phenomena in H_2," *Journal of Thermophysics and Heat Transfer*, Vol. 5, No. 4, 1991, pp. 469–480.

[14]Sharma, S. P., "Rotational Relaxation of Molecular Hydrogen at Moderate Temperatures," AIAA Paper 92-2854, July 1992.

[15]Willauer, D. L., and Varghese, P. L., "Direct Stimulation of Rotational Relaxation Using State-to-State Cross Sections," *Journal of Thermophysics and Heat Transfer*, Vol. 7, No. 1, 1993, pp. 49–54.

[16]Millikan, R. C., and White, D. R., "Systematics of Vibrational Relaxation," *Journal of Chemical Physics*, Vol. 39, No. 12, 1963, pp. 3209–3213.

[17]Chase, M. W., Jr., Davies, C. A., Downey, J. R., Jr., Frurip, D. J., McDonald, R. A., and Syverud, A. N., "JANAF Thermochemical Tables, Third Edition, Part I, Al–Co," *Journal of Physical and Chemical Reference Data*, Vol. 14, Supplement 1, 1985, p. 1260.

[18]Vincenti, W. G., and Kruger, C. H., Jr., *Introduction to Physical Gas Dynamics*, 1st ed., Wiley, New York, 1965, pp. 132.

[19]Haas, B. L., "Particle Simulation of Satellite Aerobraking with Coupled Surface Heat Transfer," *Rarefied Gas Dynamics: Space Science and Engineering*, edited by B. D. Shizgal and D. P. Weaver, Vol. 160, Progress in Astronautics and Aeronautics, AIAA, Washington, DC, 1994, pp. 44–52.

[20]Haas, B. L., "Models for Dynamic Surface Temperatures During Rarefied Aeropass Maneuvers," AIAA Paper 93-2765, July 1993.

[21]Bueche, J. F., "Effects of Improvements and Uncertainties in Thermophysical Properties on Carbon Phenolic Heatshield Thermal Performance Predictions," AIAA Paper 77-37290, June 1977.

[22]Pope, R. B., "Measurements of the Total Surface Emittance of Charring Ablators," *AIAA Journal*, Vol. 5, No. 12, 1967, pp. 2285, 2286.

[23]Peterson, D. L., and Nicolett, W. E., "Heat Shielding for Venus Entry Probes," *Journal of Spacecraft*, Vol. 11, No. 6, 1979, pp. 382–387.

[24]Pitts, W. C., and Wakefield, R. M., "Performance of Entry Heat Shields on Pioneer Venus Probes," *Journal of Geophysical Research*, Vol. 85, No. A13, 1980, pp. 8333–8337.

[25]Green, M. J., and Davy, W. C., "Galileo Probe Forebody Thermal Protection," AIAA Paper 81-1073, June 1981.

[26]Saxena, S. C., and Joshi, R. K., "Thermal Accommodation and Adsorption Coefficients of Gases," McGraw-Hill/CINDAS Data Series on Material Properties, Vol. II-1, edited by Y. S. Touloukian and C. Y. Ho, McGraw–Hill, New York, 1981, p. 188.

[27]Hollenbeck, D., and Salpeter, E. E., "Surface Adsorption of Light Gas Atoms," *Journal of Chemical Physics*, Vol. 53, No. 1, 1980, pp. 79–86.

[28]Moyer, C. B., and Rindal, R. A., "An Analysis of the Chemically Reacting Boundary Layer and Charring Ablator. Part II: Finite Difference Solution for the In-Depth Response of Charring Materials Considering Surface Chemical and Energy Balances," NASA CR-1061, June 1968.

[29]Anon., "User's Manual Aerotherm Charring Material Thermal Response and Ablation Program CMA87," Acurex Corp., Mountain View, Report UM-87-11/ATD, Aug. 1987.

[30]Hilsenrath, J., Beckett, C. W., Benedict, W. S., Fano, L., Hodge, J. H., Masi, J. F., Nuttall, R. L., Touloukian, Y. S., and Woolley, H. W., *Tables of Thermodynamic and Transport Properties*, 1st ed., Pergamon, New York, 1960, p. 245.

[31]Haas, B. L., "Flow Resolution and Domain Influence in Rarefied Hypersonic Blunt-Body Flows," *Journal of Thermophysics and Heat Transfer*, Vol. 8, No. 4, 1993, pp. 751–757.

I. D. Boyd
Associate Editor